Biochimica et Biophysica Acta 1840 (2014) 2340–2350

Contents lists available at ScienceDirect

Biochimica et Biophysica Acta

journal homepage: www.elsevier.com/locate/bbagen

Knocking down 10-formyltetrahydrofolate dehydrogenase increased oxidative stress and impeded zebrafish embryogenesis by obstructing morphogenetic movement☆

Wen-Ni Chang [a], Gang-Hui Lee [a], Tseng-Ting Kao [a], Cha-Ying Lin [b], Tsun-Hsien Hsiao [a], Jen-Ning Tsai [c], Bing-Hung Chen [d], Yau-Hung Chen [e], Hsin-Ru Wu [e], Huai-Jen Tsai [f], Tzu-Fun Fu [a,b,*]

[a] Institute of Basic Medical Science and Biotechnology, College of Medicine, National Cheng Kung University, Tainan 701, Taiwan
[b] Department of Medical Laboratory Science and Biotechnology, College of Medicine, National Cheng Kung University, Tainan 701, Taiwan
[c] School of Medical Laboratory and Biotechnology, Chung Shan Medical University, Taichung 402, Taiwan
[d] Department of Biotechnology, Kaohsiung Medical University, Kao;hsiung 807, Taiwan
[e] Department of Chemistry, Tamkang University, Taipei 106, Taiwan
[f] Institute of Molecular and Cellular Biology, National Taiwan University, Taipei 106, Taiwan

ARTICLE INFO

Article history:
Received 27 January 2014
Received in revised form 25 March 2014
Accepted 9 April 2014
Available online 18 April 2014

Keywords:
Zebrafish
ROS
Cell migration
Folate metabolism
FDH

ABSTRACT

Background: Folate is an essential nutrient for cell survival and embryogenesis. 10-Formyltetrahydrofolate dehydrogenase (FDH) is the most abundant folate enzyme in folate-mediated one-carbon metabolism. 10-Formyltetrahydrofolate dehydrogenase converts 10-formyltetrahydrofolate to tetrahydrofolate and CO_2, the only pathway responsible for formate oxidation in methanol intoxication. 10-Formyltetrahydrofolate dehydrogenase has been considered a potential chemotherapeutic target because it was down-regulated in cancer cells. However, the normal physiological significance of 10-Formyltetrahydrofolate dehydrogenase is not completely understood, hampering the development of therapeutic drug/regimen targeting 10-Formyltetrahydrofolate dehydrogenase.

Methods: 10-Formyltetrahydrofolate dehydrogenase expression in zebrafish embryos was knocked-down using morpholino oligonucleotides. The morphological and biochemical characteristics of fdh morphants were examined using specific dye staining and whole-mount in-situ hybridization. Embryonic folate contents were determined by HPLC.

Results: The expression of 10-formyltetrahydrofolate dehydrogenase was consistent in whole embryos during early embryogenesis and became tissue-specific in later stages. Knocking-down fdh impeded morphogenetic movement and caused incorrect cardiac positioning, defective hematopoiesis, notochordmalformation and ultimate death of morphants. Obstructed F-actin polymerization and delayed epiboly were observed in fdh morphants. These abnormalities were reversed either by adding tetrahydrofolate or antioxidant or by co-injecting the mRNA encoding 10-formyltetrahydrofolate dehydrogenase N-terminal domain, supporting the anti-oxidative activity of 10-formyltetrahydrofolate dehydrogenase and the in vivo function of tetrahydrofolate conservation for 10-formyltetrahydrofolate dehydrogenase N-terminal domain.

Conclusions: 10-Formyltetrahydrofolate dehydrogenase functioned in conserving the unstable tetrahydrofolate and contributing to the intracellular anti-oxidative capacity of embryos, which was crucial in promoting proper cell migration during embryogenesis.

General significance: These newly reported tetrahydrofolate conserving and anti-oxidative activities of 10-formyltetrahydrofolate dehydrogenase shall be important for unraveling 10-formyltetrahydrofolate dehydrogenase biological significance and the drug development targeting 10-formyltetrahydrofolate dehydrogenase.

Abbreviations: FDH, 10-formyltetrahydrofolate dehydrogenase; THF, tetrahydrofolate; dpf, day-post-fertilization; hpf, hour-post-fertilization; MO, morpholino oligonucleotide; WISH, whole-mount in situ hybridization; FDH-N-ter, FDH N-terminal domain

☆ Our sincere appreciation goes to Dr. Verne Schirch, Virginia Commonwealth University, for his valuable advice and assistance. We acknowledge the support from the following grants: NSC 96-2320-B-006-023-MY3 funded by the National Science Council Taiwan. We also thank Taiwan Zebrafish Core Facility at ZeTH (supported by NSC grant 101-2321-B-400-014) for the material and technical support.

* Corresponding author at: Department of Medical Laboratory Science and Biotechnology, College of Medicine, National Cheng Kung University, No. 1, University Road, Tainan 701, Taiwan. Tel.: +886 6 2353535x5795; fax: +886 6 236 3956.
E-mail address: tffu@mail.ncku.edu.tw (T.-F. Fu).

http://dx.doi.org/10.1016/j.bbagen.2014.04.009
0304-4165/

1. Introduction

Folate is a B vitamin essential for embryonic development and heavily involved in the metabolism of many fundamental biomolecules, including purines, choline, amino acids, neurotransmitters and S-adenosylmethionine (SAM), the major methyl donor for most intracellular methylation reactions. Insufficient folate has been associated with many congenital anomalies including heart and neural tube defects [1]. In cells, tetrahydrofolate carries a one-carbon unit at either the N5 and/or N10 positions, forming different folate adducts. These folate adducts participate in one-carbon metabolic (OCM) pathways and are interconverted via several redox and synthetic reactions catalyzed by several folate enzymes. Among all the folate enzymes participating in this pathway, 10-formyltetrahydrofolate dehydrogenase (10-formyltetrahydrofolate:$NADP^+$ oxidoreductase; FDH or ALDH1L1; E.C.1.5.1.6) is the most abundant one, comprising 1% of total soluble protein in the rabbit liver [2]. FDH catalyzes the conversion of 10-formyltetrahydrofolate (10-formyl-THF) to tetrahydrofolate (THF) and CO_2 (Eq. 1). Therefore, FDH was proposed to regulate the ratio of these two major intracellular reduced folate pools.

Mammalian FDH is a homotetramer consisting of four identical 99 kD subunits. Each subunit is composed of a large C-terminal domain and a small N-terminal domain connected by a linking peptide. The proper alignment to bring both N- and C-terminal domains in a correct orientation is required for 10-formyltetrahydrofolate dehydrogenase activity [3]. The large C-terminal domain contains a $NADP^+$ binding site and has aldehyde dehydrogenase activity (Eq. 2) [2,4]. This aldehyde dehydrogenase activity was not found in zebrafish FDH [5]. The small N-terminal domain contains a 10-formyl-THF binding site and catalyzes a 10-formyl-THF hydrolysis reaction (Eq. 3). The physiological significance of this hydrolase activity remains unclear. One proposal is that this $NADP^+$-independent hydrolase activity is to produce THF irrespective of the redox state (NADPH/$NADP^+$ ratio) in the cell [6]. On the N-terminal domain also resides a non-catalytic THF tight binding site, which partially overlaps with the substrate catalytic site [7]. Currently, the function of this non-catalytic site is unknown.

$$\text{10-formyl-THF} + NADP^+ \rightarrow \text{THF} + CO_2 + \text{NADPH} \quad (1)$$

$$\text{Propanal} + NADP^+ \rightarrow \text{propanoate} + \text{NADPH} \quad (2)$$

$$\text{10-formyl-THF} \rightarrow \text{THF} + \text{formate} \quad (3)$$

The physiological significance of FDH is not completely understood. The clinical importance of FDH was first recognized in methanol detoxification, in which FDH is responsible for the ultimate removal of formate [8]. However, this could not be considered an adequate reason for FDH to exist in such a high quantity, leaving the biological significance of FDH under normal physiological conditions an unanswered question. Sequestering unstable THF for storage and regulating free THF availability is one of the functions postulated for FDH [9,10]. The specific expression of FDH in the radial glia at the midline of neural tube during murine embryogenesis suggested a role for FDH in neural tube formation, although loss-of-function FDH mutations did not impair neural tube closure [11]. Homozygous mice lacking FDH appeared completely normal but exhibited a reproductive deficiency, which was attributed to a possible increase of fetal lethality [12]. Recently, overexpressing FDH has been shown to evoke metabolic stress and cause apoptosis in cancer cells, shedding light on the possibility of FDH being a chemotherapeutic target [13–15]. Nevertheless, the biological significance of FDH remains incompletely understood, especially under normal physiological condition, hampering the development of therapeutic drug/regimen targeting FDH.

Zebrafish has been a prominent vertebrate model for biological and medical research. Considering its features of transparent embryos, external and rapid development and high throughput, zebrafish could serve as a valuable complementary in vivo platform for folate-related studies. Several zebrafish folate enzymes, including FDH, had been characterized and shown to resemble mammalian orthologs, supporting the use of zebrafish to model folate-mediated one-carbon metabolism [5, 16–21]. In this study, we report the spatially specific but temporally constant expression of FDH during embryogenesis. We examined the biological significance of FDH in develo\ping embryos using knock-down strategies. The potential physiological function of FDH is also discussed.

2. Materials and methods

2.1. Materials

The SMART™ RACE amplification kit was purchased from Clontech, Inc. (California, US). Enzymes used for cloning were purchased from New England BioLabs, Inc. (Maryland, US). The HPLC gel filtration column Alltech ProSphere SEC, 250 HR, S-200 (4.6 mm × 30.0 cm) was purchased from Alltech (Illinois, US). 10-Formyl-5,8-dideazafolate-ω-Aminohexyl-Sepharose 4B affinity column was prepared as previously described [2]. Horseradish peroxidase-conjugated goat anti-rabbit IgG secondary antibody was purchased from Santa Cruz Biotechnology Inc. (California, US). Folates were generous gifts from Dr. Moser (Merck Eprova AG, Switzerland). The AB strain zebrafish embryo was a generous gift from Dr. Hans Georg Frohnhöfer (Max-Planck-Institut für Entwicklungsbiologie, Tübingen, Germany). The cRNA expression vector pcGlobin2 was a gift from Dr. Myungchull Rhee (Chungnam National University, Daejeon, Korea). All other chemicals, including coenzymes, buffers, amino acids, and antibiotics, were purchased from Sigma-Aldrich Chemical Co. (Montana, US). The *Escherichia coli* strains and vectors used for cloning and protein expression have been described previously [5].

2.2. Fish care and sample preparation for Western blot and RT-PCR analysis

Zebrafish (*Danio rerio*, AB strain) were bred and maintained in a 14–10 h light–dark diurnal cycle following the standard procedure [22]. Embryos were staged according to Kimmel et al. [23]. The animal studies and all procedures for handling zebrafish and embryos, including breeding and maintenance of fish and sample collection, were approved by Affidavit of Approval of Animal Use Protocol of National Cheng Kung University (IACUC Approval NO. 96062). Embryos and tissues obtained from adult zebrafish were prepared for Western blot analysis and RT-PCR to determine cytosolic FDH (CFDH) levels and distribution as previously described [18]. The dominant yolk proteins in embryos before 24-hpf were removed for Western blot analysis to avoid interference [24]. The purified rabbit anti-zebrafish cytosolic FDH-N antibody was used at 1:500 dilutions. Rabbit anti-actin antibody was used as a loading control. The primer pairs used for RT-PCR were as follows: 5′-CGCTGAGC ATATGAGGGTGGTG-3′(forward) and 5′-GGTATAGACTGCTCCCGAG-3′(reverse) for zebrafish CFDH (570-bp fragment) and 5′-AGACATCA AGGAGAAGCTGTG-3′(forward) and 5′-TCCAGACGGAGTATTTAC-3′(reverse) for β-actin (391-bp fragment) as a control for the RNA isolation and reverse-transcription.

2.3. Whole mount F-actin staining

Embryos were fixed overnight in 4% paraformaldehyde at 4 °C. Embryos were washed in 0.1% PBSTx and dechorionated. They were then incubated for 1 h in 0.5% PBSTx, followed by 4-hour incubation in blocking buffer (PBS, 1% BSA, 10% goat serum, 1% DMSO, 0.1% Triton X100). Embryos were then incubated overnight at 4 °C in blocking solution containing phalloidin or primary antibody. Alexa 488 phalloidin (molecular probe) was used at 1:400 dilutions. Images were observed under a multi-photon confocal microscope (Olympus) and acquired with the software FluoView FV1000.

2.4. Cytosolic FDH knockdown, cRNA injection and rescue

The sequences of MOs designed by the manufacturer (GeneTools, LLC, Philomath, OR), based on the *cfdh* mRNA sequence we provided, were: MO1 (5′-TCTTTGCACGTCCCAATAAGAGCCG-3′) and MO2 (5′-TTCCTCTGCACGAAAGAAAGATTCA-3′) (Fig. S1). Complete coding sequence or only N-terminus domain (amino acid 1–311) of zebrafish cytosolic FDH was cloned into pcGlibin2 by EcoRI restriction enzyme sites [20]. The plasmid was linearized by XbaI and transcribed in a reaction mixture containing T7 RNA polymerase (Roche), GpppG cap analog (New England Biolabs), NTP and RNasin (Promega) at 37 °C for 2 h. The synthesized *cfdh* cRNA was purified by phenol–chloroform extraction and quantified by absorbance at 260 nm on a Helios spectrophotometer (Thermo). All reagents for microinjection, including MO, capped-mRNA and folates, were dissolved in degassed and RNase free Danieu's buffer to make proper stock solutions.

For microinjection, approximately 4.6 nl of solution containing MO, capped-mRNA and/or folate was injected into embryos at the 1 to 4-cell stages to reach the desired concentrations. For rescue experiments, embryos were incubated in embryo's medium containing 0.25 mM THF or 20 μM N-acetyl-L-cysteine (NAC). Embryos injected with Danieu's buffer and standard control MO served as injection controls in each experiment. Each experiment was repeated at least four times with approximately 50 embryos used for each group.

2.5. Whole-mount in situ hybridization (WISH)

WISH with digoxigenin (DIG)-labeled riboprobes was performed following the protocol described by Jowett [25] and Thisse [26]. Riboprobes were generated by in vitro transcription in the presence of digoxigenin-11-UTP from linearized templates. The probe used for *fdh* was generated from a linearized plasmid containing the partial coding sequences and 3′ UTR of zebrafish *fdh*.

2.6. Folate detection

Individual folate adducts in embryos were measured following the protocols as previously described [19]. In brief, approximately 50 embryos were homogenized in 0.3 ml of extraction buffer flushed with nitrogen and heated in boiling water for 5 min before centrifugation. Conversion of folyl polyglutamates in the supernatant to folate monoglutamates was achieved by incubating the embryo extracts with 2 μg of purified recombinant zebrafish gamma-glutamyl hydrolase and incubated at 37 °C for 5 min. After centrifugation and filtration, 50 μl of the clear supernatant was injected into an Aquasil C_{18} column on an HPLC system (Agilent 1100) for folate detection. The potential folate peaks in extracts were identified by overlapping the retention times between the prospective folate peaks and folate standards.

2.7. Hemoglobin

Embryonic hemoglobin was visualized by incubating de-chorionated embryos in O-dianisidine (0.6 mg/ml) solution in the dark for 15 min as previously described [27]. Presence of brown coloration indicates erythrocytes containing hemoglobin (Hb). Embryos were post-fixed in 4% paraformaldehyde/PBS overnight at 4 °C and observed under light dissecting microscope.

2.8. Cell proliferation, apoptosis and neuromast staining

Cell proliferation was evaluated with BrdU incorporation by incubating dechorionated embryos in 10 mM BrdU solution at 16 °C for 30 min [28]. Apoptotic cells were visualized by incubating lived embryos in 1 μM YO-PRO-1 (Invitrogen/Molecular Probes, Eugene, OR) solution at 4 °C for 1 h in the dark and observed under a fluorescence dissecting microscope (excitation 491 nm, emission 509 nm) after a thorough wash [29]. Hair cells in lateral line neuromasts were labeled by incubating embryos in 5 μM 4-(4-diethylaminostyryl)-N-methylpyridinium iodide (4-Di-2-ASP) for 10 min and then observed under a fluorescence dissecting microscope (excitation 488 nm, emission 607 nm) after being washed and anesthetized with tricaine.

2.9. Reactive oxygen species (ROS) assay

Reactive oxygen species (ROS) accumulation was assessed by incubating dechorionated embryos in 100 μM solution of a non-fluorescent dye 2′,7′-dihydrodichlorofluorescein diacetate (H2DCFDA) for 30 min. H2DCFDA was oxidized by ROS to generate dichlorofluorescein (DCF) [30], which was fluorescent and observed with a Leica Z16 APO fluorescence dissecting microscope (excitation 485 nm, emission 560 nm).

2.10. Alcian blue cartilage staining

Embryos of 4 dpf were fixed overnight in 4% paraformaldehyde at 4 °C. After being washed thoroughly in PBS then dehydrated gradually in ethanol and embryos were stained in 0.1% Alcian blue solution (in acetic acid) at room temperature overnight [31]. Embryos were rinsed in 100% ethanol and serially rehydrated in PBS. Further translucentization of the tissue was achieved by incubating embryos in 0.05% trypsin, 1% KOH and 3% hydrogen peroxide solutions sequentially. Embryos were washed in PBS and mounted in 80% glycetrol–2% KOH.

3. Results

3.1. Distribution of FDH was spatially dependent and tissue-specific

The distribution of FDH in adult zebrafish was tissue specific in both protein and mRNA levels. FDH was most abundant in the liver and then in the GI and spinal cord of adult fish (Fig. 1A). In contrast, both *fdh* mRNA and protein were equally distributed in embryos of all examined stages during embryogenesis (Fig. 1B). The presence of mRNA in embryos before 3 hpf implied a maternal deposition of maternal *fdh* mRNA since the zygotic transcription did not begin until 3 hpf [32]. The results of whole-mount in-situ hybridization (WISH) revealed a spatially and temporally specific expression of *fdh* in early embryos. *Fdh* transcripts were evenly distributed in embryonic epiblasts at 6 hpf but gradually focused in the floor plate and head region, including eyes and mid-hindbrain boundary, as embryogenesis proceeded (Fig. 1C). The *fdh* signal was initially detected in polster, a tissue crucial for embryonic patterning, and became abundant in somites and intermediate cell mass (ICM) in 24 hpf embryos (Fig. 1C-b–f). *Fdh* was expressed, apparently and almost exclusively, in the embryonic liver and gastrointestinal tract by 3 dpf (Fig. 1C-g). The expression of *fdh* was continuously focused on the larval liver and digestive tract at least up to 5-dpf (Fig. 1D). The agreement in the temporal and spatial distributions between *fdh* expressed protein and mRNA levels indicates that transcriptional regulation might contribute considerably to expressional control. The constant expression of *fdh* during embryogenesis also suggests a role for FDH in zebrafish embryogenesis.

3.2. Fdh morphants exhibited defective embryogenesis

The strategy of using an antisense morpholino oligonucleotide (MO) to block gene translation has been widely used to determine gene function in vivo [33]. Two non-overlapping *fdh*-MOs, MO-1 and MO-2, were injected into embryos at 1 to 2-cell stages and dose-dependently decreased *fdh* protein translation (Supplement 1). Both MO-1 (9.6 ng) and MO-2 (4.8 ng) exerted an approximately 40 to 60% decrease in FDH protein level and caused comparable morphological abnormalities in morphants (Fig. 2 and Supplement 1B). To avoid redundancy, only the results of MO-2 were presented in the current report and described as “MO” in the subsequent discussion unless otherwise indicated.

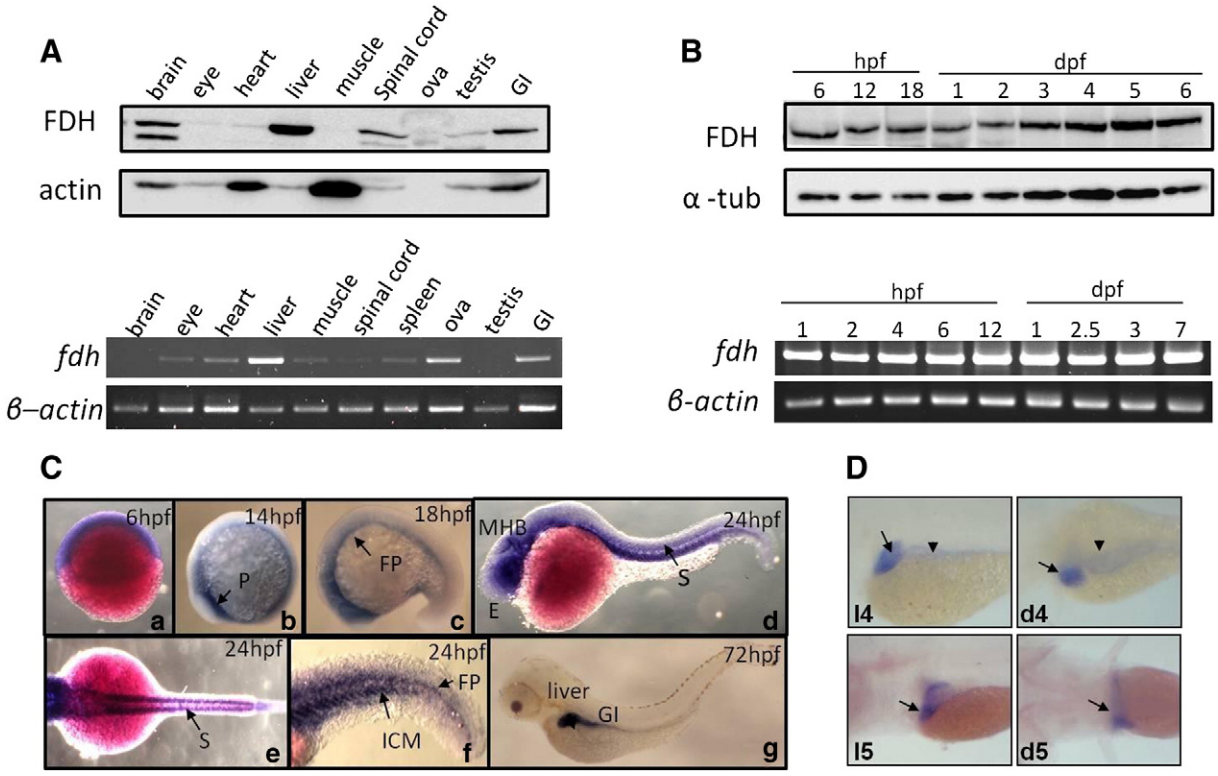

Fig. 1. Distributions of FDH in zebrafish adult and embryos. Individual tissues of adult female zebrafish (A) and embryos at the indicated stages (B) were subjected to Western blot analysis (top) and RT-PCR (bottom) for FDH distribution. 20 μg protein was used for each lane. Results presented are representative of seven independent repeats. (C) Embryos probing with fdh anti-sense RNA for WISH revealed a homogenous distribution in embryos at 6 hpf and specific expression in neural tissues, somites, liver and GI, in embryos of later stages. (D) The WISH signals for *fdh* were focused in the liver (arrow) and GI (arrowhead) of embryos at 4-dpf (l4 and d4) and 5-dpf (l5 and d5). Most embryos are shown in lateral view with anterior to the left except in C—e, D—d4 and D—d5, which are shown in dorsal view. P, polster; FP, floor plate; GI, gastrointestinal tract; ICM, intermediate cell mass of mesoderm; MHB, mid–hindbrain boundary.

Embryos injected with a scrambled MO displayed normal morphology and served as the control for the knockdown procedure. Defective embryonic development, including malformed heart and trunk, was observed in embryos injected with *fdh* MOs (*fdh* morphants or morphants) at 2 dpf and became increasingly evident at 3-dpf. Morphants at 3 dpf were categorized into the groups of normal, mild and severe based on the severity of gross morphological anomaly (Fig. 2B). The quantification for morphants in each group revealed significant impact to embryonic development. Morphants displayed a thin and tubing heart accompanied by pericardial edema and lowered heart rate, a shortened yolk extension, diminished circulating blood cells, curved body with shortened trunk, atrophic tail and kinked notochords (Fig. 2B and Supplements 2 and 3). Distorted heart with a tube-shape suggested an unsuccessful looping, which was seen more clearly in the *fdh* morphant of Tg(*cmlc2:egfp*) embryos with EGFP expression in the myocardial cells [34]. Control embryos had completed the majority of the heart looping process and possessed a compacted and functional heart with a distinct ventricle and an atrium at 48 hpf (Fig. 2C). However, the heart tube of *fdh* morphants remained in tube-shaped midline structures, confirming uncoupling of D-looping (the subsequent repositioning of the ventricle to the right of the atrium). Circulating blood cells were significantly decreased in more than 65% of *fdh*-morphants. The interfered circulation was confirmed by O-dianisidine staining for hemoglobin, in which reduced hemoglobin signal and ectopic accumulation of blood cells in extravascular tissues were observed (Fig. 2D). Smaller head and eyes were also noticed, suggesting craniofacial malformation in *fdh* morphants. Subsequent Alcian blue staining of 4 dpf *fdh* morphants for larval cartilage revealed distorted Meckel's cartilages and ceratohyal angle. The ceratobranchial cartilages in *fdh* morphants were also disappeared, confirming impeded craniofacial development (Fig. 2E).

To ensure the knockdown specificity, *fdh* mRNA and THF were co-injected with MO for rescue (Fig. 2 and Supplements 2 to 7). Partial reversal in the severity of abnormal gross morphology was observed in *fdh* mRNA (f-R) co-injected morphants. Successful heart looping and increased heart rate were observed in the rescued embryos. Blood cells re-appeared although extravascular blood cells accumulation occurred occasionally due to the still-slower-than-normal heart rate. Unexpectedly, co-injecting the mRNA encoding only the *fdh* N-terminal domain (fN-R) also exerted an effective rescue (Fig. 2B). Exposing *fdh* morphants to THF, the catalytic product of FDH, significantly alleviated the morphological abnormalities (Fig. 2, Supplements 5 to 6). Co-injecting p53 MO for suppressing non-specific knockdown off-target effects did not change the severity observed in *fdh* morphants (Supplement 7). Our results suggested that *fdh* was crucial for embryonic development.

3.3. Knocking-down FDH impeded the formation of various embryonic tissues at early developmental stages

Fdh morphants before 24 hpf were subjected to WISH and compared with control embryos for tissue formation. In morphants, the expression domain of *ntl*, which represents chorda mesoderm (the notochord rudiment) in the dorsal midline, was shorter and wider and failed to extend to the anterior end of embryos, indicating an affected notochord (Fig. 3, a–a2). The distortion of the notochord was more evident at the tail region at 22 hpf (Fig. 3, b–b2). Mis-shaped neuroectoderm (*krox20* and *pax2.1*) in the mid–hind brain boundary, optic vesicle and rhombomeres with reduced signals also appeared (Fig. 3, c–c2, d–d2, e–e2 and f–f2). Widened distance between bilateral adaxial cells, the precursors to the embryonic slow muscle fibers, was also obvious when probed with the mesoderm marker (Fig. 3, g–g2 and h–h2).

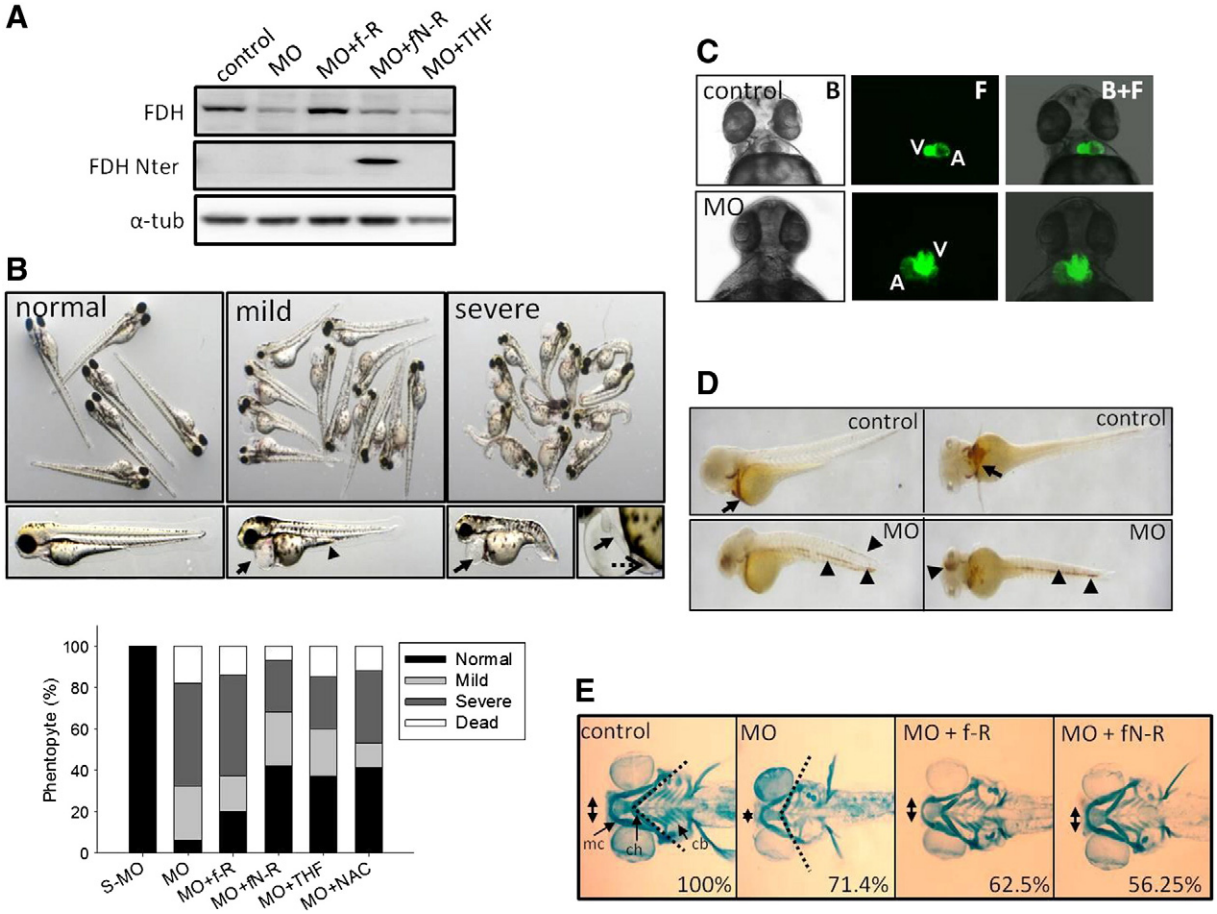

Fig. 2. The impact of knocking-down fdh to zebrafish embryonic development. Embryos at 1 to 4-cell stage were injected with 4.8 ng of scramble MO or zebrafish *fdh* MO and monitored for embryonic development at 3 dpf. (A) Embryos injected with scramble MO (control), *fdh* MO (MO), *fdh* MO plus 400 pg *fdh* full-length mRNA (MO + f-R), *fdh* MO plus 400 pg *fdh* N-terminal mRNA (MO + *f*N-R) or *fdh* MO plus 5 pmol THF (MO + THF) were examined for FDH protein level with Western blotting using anti-zebrafish FDH N-ter antibody. (B) (upper) Morphants were categorized into the categories of normal, mild and severe based on the severity of phenotypic abnormality: normal, embryos with correctly looped and functional heart and straight body trunk; mild, embryos with pericardial edema and distorted heart chambers, lowered heart rate and/or mild curved trunk; severe, pericardial edema with unsuccessfully looped heart tube, significantly decreased heart rate (<20 beats/min) and/or curved/shorten body trunk. Enlarged or tube-shaped cardiac chambers lacking flowing blood cells (the inset of higher magnitude with arrow) were often observed in morphants, especially in severe group. Abnormally accumulated blood cells in bulbus arteriosus (dotted arrow) and shortened yolk extension (arrowhead) also appeared. Body curvature was evident in severe group. (lower) The percentages of embryos with the distinct phenotypes were quantified. Data were reported in average of at least eight independently performed experiments. Approximately 40–60 embryos were included in each experiment for each group. (C) Tg(*cmlc2*-eGFP) embryos injected with 4.8 ng MO exhibited unsuccessful looping of heart tube in comparison to control embryos. Ventral to dorsal view at 48 hpf. V, ventricle; A, atrium. B + F, merged image of both bright and fluorescent images. (D) Significantly decreased signal of O-dianisidine staining in sinus venosus (arrow) and ectopic accumulation of red blood cells in peripheral extravascular tissues (arrowhead) were observed in *fdh* morphants (MO). (E) Morphants at 4 dpf were examined for their craniofacial structures with Alcian blue staining. Distorted Meckel's cartilages (double-headed arrow) and ceratohyal angle (dotted line) were apparent in fdh morphants, as well as the disappearance of ceratobranchial. Embryos are viewed from ventral to dorsal with anterior to the left. The percentage of morphants displaying the presented phenotype is indicated at the lower-right corner. mc: Meckel's cartilage; ch: ceratohyal cartilage; cb, ceratobranchial.

Unlike the chevron-shaped somites observed in control embryos, rounded somites appeared in *fdh* morphants. These results indicated that the axial tissues, including the axial and paraxial mesoderm, fail to extend and converge properly in *fdh* morphants. The misplaced *cmlc2* signals in 24-hpf morphants were consistent with the defective heart observed in 3 dpf morphants (Fig. 3i–i2). The lack of *c-myb* signal in morphants at the posterior blood island, the caudal hematopoietic tissues of zebrafish embryos, also echoed the absence of circulating blood cells observed in the heart of *fdh* morphants at 3 dpf (Fig. 3j–j2). These results showed that *fdh* knock-down profoundly impeded the origin of embryonic tissues at rather early stages.

3.4. Reduced FDH expression impeded morphogenetic movement

The observation that knocking down *fdh* expression caused defects in a wide-spectrum of tissues implied affected primordial neural crest cells. Neural crest cells are a collection of cells that appears near the dorsal margins of the closing neural tube, which disperse throughout the body of embryos where they give rise to a variety of structures including the teeth, bones, cartilage, skin, sensory capsules involving eyes and other sense organs. Probing both control embryos and *fdh* morphants of early stages with neural crest (NC) cell markers for WISH revealed interfered NC cells patterning in morphants. Both control embryos and *fdh* morphants displayed comparable signal intensities for NC cell markers before 18 hpf except the slightly decreased *Bmp 4* and *msxE* at the polster (Fig. 4, a–a2 and b–b2). These results suggested that the primordial induction and specification for NC cells were mostly unaffected at early embryonic stages. However, the patterning of NC cell markers was altered. In comparison to control embryos, *fdh* morphants at 12 hpf displayed a widened space between the neural plate edges stained by *snai 1b* and *sox10* (Fig. 4, c–c2 and d–d2). In control embryos at 16–18 hpf, *sox10* positive NC cells migrated ventrally from the dorsal aspect of the neural tube in bilateral streams to the otic vesicle and the preotic and postotic clusters of glial precursors (Fig. 4f′, arrowhead). However, those ventrally and bilaterally migratory NC cells were not observed in *fdh* morphants. Instead, NC cells aggregated at the dorsal midline (Fig. 4, f1 and f2, arrow). The expression of *snai 1a*, which is specific to segmental plate and tail bud, was comparable

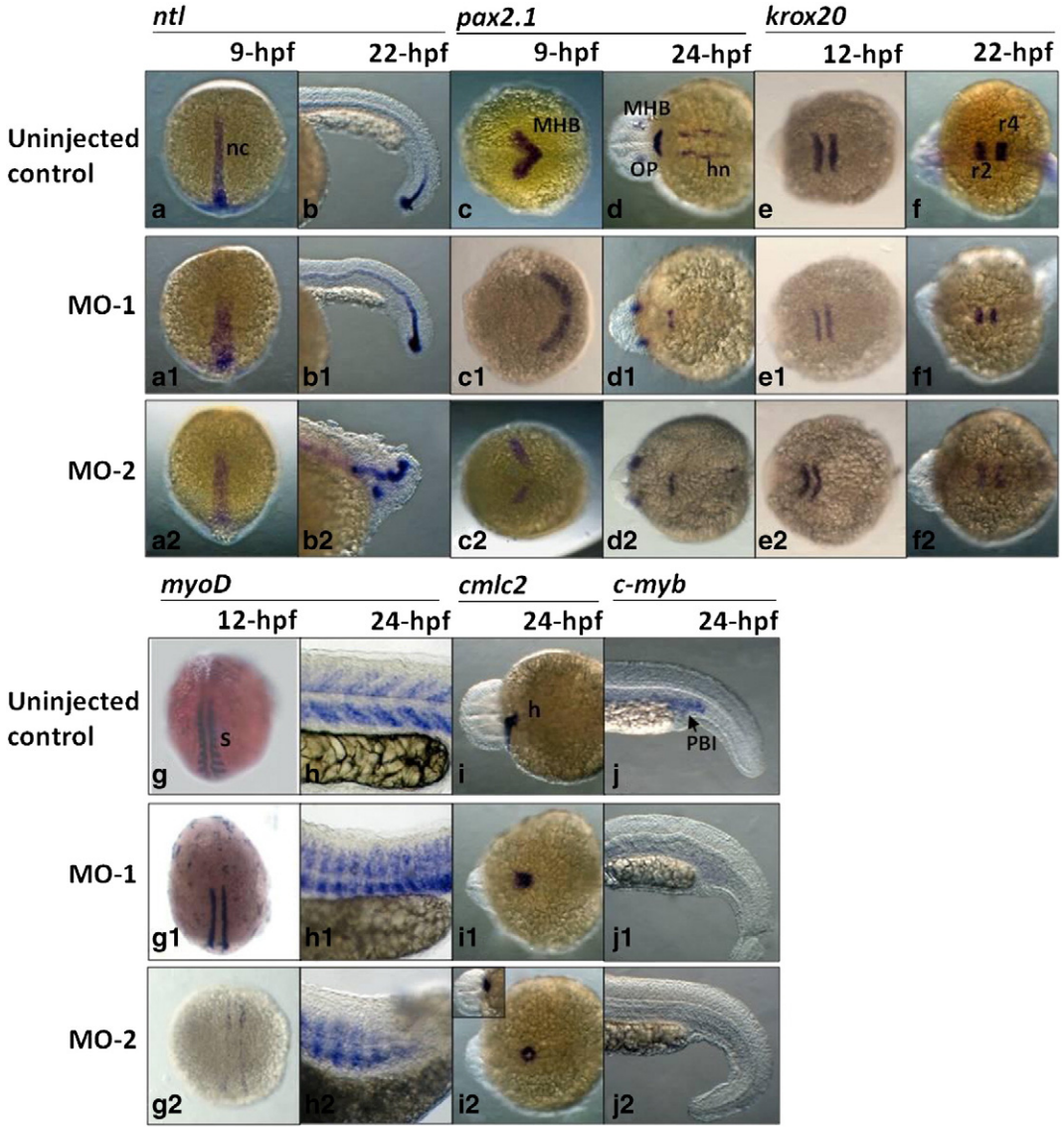

Fig. 3. The effects of reduced fdh expression in embryonic tissue formation. Embryos of uninjected control (a–j) and those injected with 4.8 ng of *fdh* MO-1 (a1 — j1) or *fdh* MO-2 (a2–j2) at 1 to 4-cell stages were collected at indicated time and subjected to WISH with probes specific for neural primodium (*krox20*: hindbrain rhombomeres; *pax2.1*: midbrain–hindbrain boundary), notochord (*ntl*), somite (*myoD*), heart (*cmlc2*) and caudal hematopoietic tissue (*c-myb*). Presented here are the representatives of the abnormal morphology which were not observed in control embryos but were apparent in MO groups. The rate of occurrence for the abnormal morphology ranged from 40% to 75%, depending on the probes used. nc, notochord; hn, hindbrain neurons; MHB, midbrain–hindbrain boundary; OP: optic stalk; r2 and r4, hindbrain rhombomeres; s, somite; h, heart; PBI, posterior blood island.

in both intensity and distribution pattern between control embryos and morphants. This observation indicated that embryos in both control and morphant groups had reached similar developmental stages and the anomalies observed in morphants should not be due to developmental delay. Taken together, our results showed that reducing *fdh* expression impeded NC cells patterning possibly by interfering NC cell migration.

3.5. Knocking down fdh expression impeded F-actin polymerization at the blastoderm margin and caused epiboly delay

A shortened body axis is a hallmark of interfered epiboly. Epiboly is the morphogenetic movement of the blastoderm starting at late blastula and followed by the conversion and extension of marginal blastomeres during gastrulation. A delayed epiboly was observed in morphants before 15 hpf. This delay was apparent as early as 7 hpf (onset of gastrulation) and became increasingly evident by 9-hpf (late gastrulation) (Fig. 5A). In control embryos, the blastoderm completely covered the yolk cell and somites began to form by 11 hpf; whereas most *fdh*-morphants still remained at 90% epiboly or earlier, leaving an unclosed yolk plug at the vegetal pole (Fig. 5A, b3 and c3). Co-injecting *fdh*-mRNA partly reversed the delayed epiboly, confirming the knockdown specificity (Fig. 5B). Again, co-injecting *fdh* N-terminal domain mRNA effectively reversed the delayed epiboly, suggesting that the N-terminal domain of FDH has folded into a stable protein with a biological function. Incubating morphants in 0.25 mM THF slightly reversed the delayed epiboly although the rescuing effect was less significant than that of fdh mRNA co-injection. Our results showed that FDH was crucial for proper morphogenetic movement during zebrafish gastrulation.

The movement of blastomeres in the enveloping layer (EVL) proceeds in the manner of collective cell migration and highly depends on a functional cytoskeleton. Microfilament networks are enriched in the cortex of EVL cells, which is especially apparent at the lamellipodial extensions in the epiblasts at the margins approaching yolk syncytial layer (YSL), and actively participates in early epiboly [35,36]. *Fdh* morphants at 75% epiboly were stained in situ with fluorescent phalloidin, a high-affinity probe specifically labeled F-actin. The actin-

enriched outer epithelium at the frontier of migrating enveloping epiblasts along the EVL margin was clearly observed in control embryos; whereas this actin-enriched boundary was significantly diminished in *fdh* morphants, suggesting a connection between the interfered F-actin formation and delayed epiboly (Fig. 5C). The actin-enriched cortical belt at the migrating EVL margin reappeared when morphants were rescued with *fdh* mRNA, confirming the causal effects of obstructed F-actin formation to the delayed epiboly caused by *fdh* knockdown.

The development of posterior lateral lines (pLL), a sensory system of teleost fish and amphibians, was significantly impeded in *fdh* morphants. A posterior lateral line comprises a set of regularly spaced neuromasts arranged in line on the body surface of zebrafish and is closely related to our auditory system. During embryogenesis, the neuromasts of pLL are deposited by proliferating and migrating primordial cells originating from cephalic placodes along the horizontal myoseptum to the tip of the tail, also in the manner resembling collective cell migration [37,38]. Embryos at 3 dpf were stained with 4-Di-2-ASP, a dye specifically accumulating in hair cells in neuromasts. The neuromasts in the posterior trunk of *fdh* morphants were significantly decreased in number or even completely disappeared (Fig. 5D). The presence of ectopically located neuromasts in *fdh* morphants indicated that the generation and differentiation of neuromast cells in *fdh* morphants were most likely intact, but the migratory polarity of the cells was lost. Again, co-injecting *fdh* mRNA or supplemented with THF reversed the disturbed neuromast distribution, confirming the specificity and causal effect of *fdh* knockdown to pLL formation and embryonic primordial cell migration.

3.6. Knocking down fdh expression increased oxidative stress and activated pERK in morphants

THF is the catalytic product of FDH and also a prominent intracellular anti-oxidant [39,40]. Examining the oxidative stress in embryos of 9 hpf and 24 hpf with DCFDA staining revealed an elevated fluorescence intensity in morphants, as compared to control embryos (Fig. 6A). This increased oxidative stress was alleviated by incubating morphants in embryo water containing THF or anti-oxidant NAC. Incubating *fdh* morphants in embryo water containing NAC also exerted rescuing effects for the phenotypic anomalies observed at later stages (Figs. 5B, D and 6B). Examining the folate content of *fdh* morphants with HPLC revealed a 40% decrease of THF levels in morphants, which was partly reversed by simultaneously co-injecting *fdh* mRNA. These results supported the causal effect of decreased THF to the elevated oxidative stress due to *fdh* knockdown. Again, co-injecting *fdh* N-ter mRNA with *fdh* MO also increased morphant THF level and reversed morphant abnormalities (Figs. 5 and 6). Injecting *fdh* mRNA alone to wild type embryos caused no appreciable difference in gross morphology, but led to an approximately 35% increase in THF level (Fig. 6C and Supplement 7). Curiously, altering *fdh* expression levels by either knockdown or overexpression did not significantly affect the embryonic 10-formyl-THF level as compared with un-injected control embryos. Together, these results indicated that it was the decreased THF level, but not 10-formyl-THF, involved in the pathological mechanism in *fdh* morphants. Also, the N-terminal domain of FDH might possess biological activities partly overlapping with full-length FDH in vivo.

Western blotting on the extracts prepared from 1 dpf morphants revealed an increased level of phosphorylated ERK, suggesting the involvement of ERK signaling in *fdh* knockdown-induced pathogenesis (Fig. 6D). Adding THF and NAC reversed the increased phospho-ERK level in *fdh* morphants, implying that the ERK activation was in response to the oxidative stress induced by the decreased embryonic THF. Also, adding U0126, a phosphor-ERK inhibitor, to embryonic water reduced the severity of phenotypic abnormity observed in *fdh* morphants (Fig. 6B). These results suggested that the ERK activation in morphants was caused by the oxidative stress due to the decreased THF and was at least partly responsible for the anomalies induced by *fdh*-knockdown.

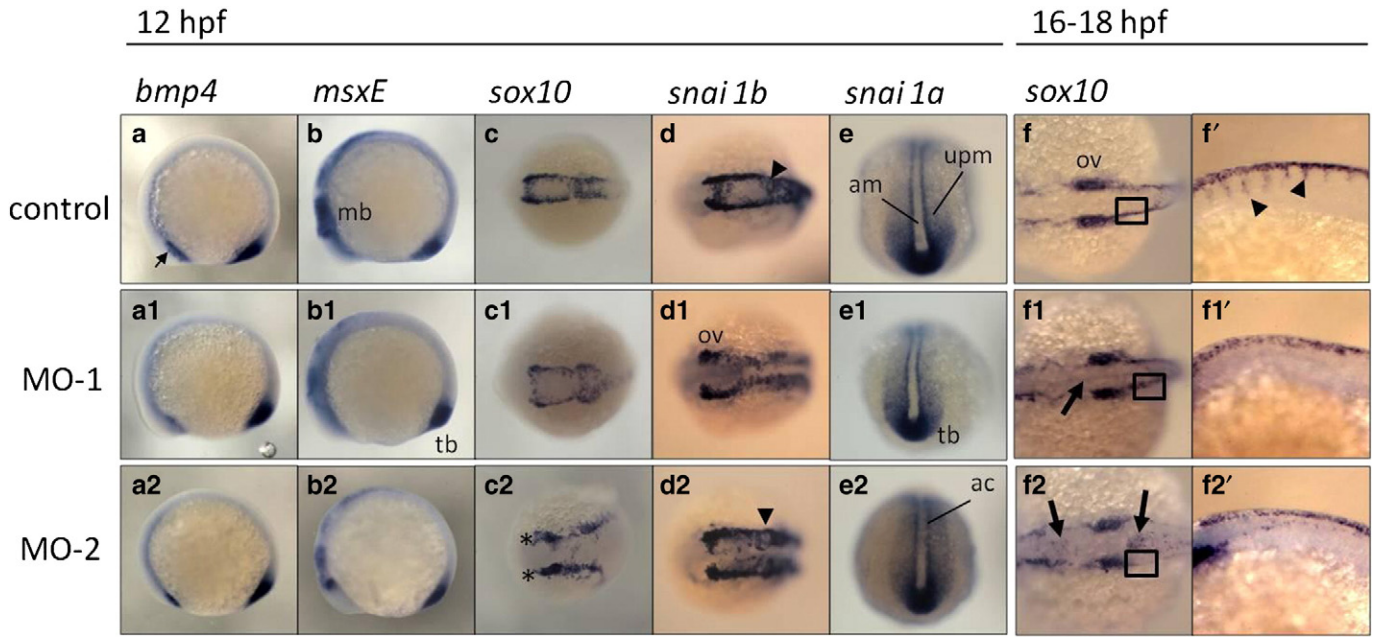

Fig. 4. The effects of reduced FDH expression in neural crest cell distribution. Embryos were examined with WISH using probes specific for neural crest primordium to evaluate the evolvement of neural crest cells and descendant tissues. Slightly decreased signal of bmp4, which labels polster (the hatching gland rudiment) underlying the forebrain during the early segmentation period, was observed in both control embryos and morphants (a–a2). Reduced intensity was observed in morphants for msxE, the marker for ectoderm, midbrain neural rod and keel, neural plate, presumptive cephalic mesoderm, optic primordium and tail bud (b–b2). Embryos were shown in lateral view with anterior to the left. *Sox10* labeled the primordial cranial neural crest precursors in embryos at 12 hpf (c–c2) and the migratory neural crest cells (f′, arrowhead), otic vesicle and the preotic and postotic clusters of glial precursors at 16–18 hpf (f–f2). f′, f1′ and f2′ show the enlarged lateral view of the boxed region in f, f1 and f2, respectively. Accumulation of neural crest cells in midline was observed in *fdh* morphants (f1 and f2, arrow). Snai 1b transcripts were observed in the otic vesicles, trigeminal ganglia (arrowhead) (d–d2). The similar patterns of *snai 1a* signals observed between control and morphants confirmed the comparable developmental stages between the compared embryos (e–e2). mb, midbrain; am, axial mesoderm ac, adaxial cells; upm, unsegmented paraxial mesoderm; tb, tail bud; ov, otic vesicle; *, anterior limit of cranial neural crest cells.

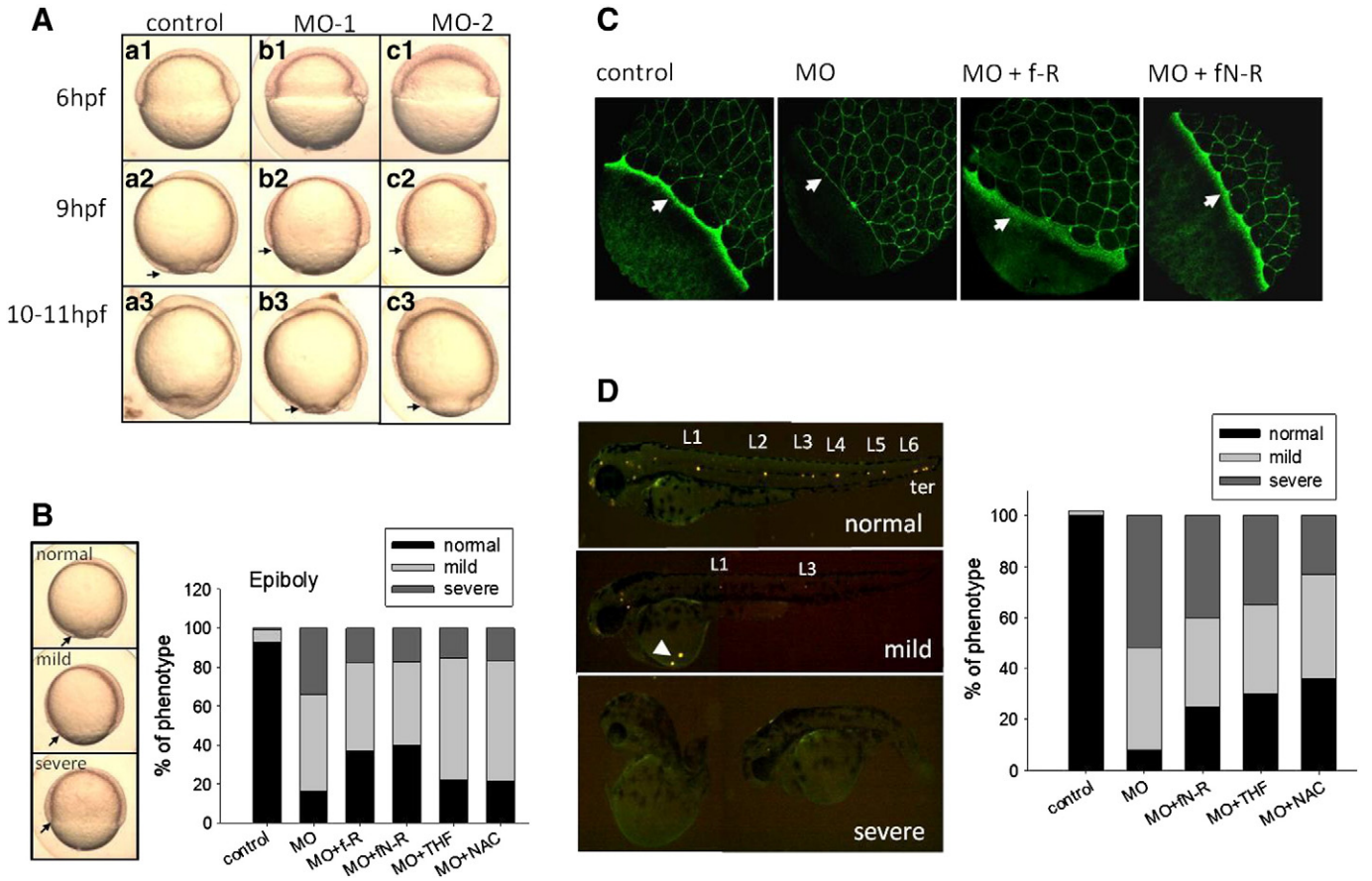

Fig. 5. Reduced *fdh* expression hindered epiboly and lateral line formation. (A) Embryos injected with *fdh* MO at 1 to 4-cell stages were examined for epibolic progression at indicated stages. FDH morphants failed to close the yolk plug by 11 hpf. Arrows indicate the leading edge of migrating marginal blastomeres. (B) FDH morphants at 9 hpf were categorized into normal (>90%), mild (75 to 90%) and severe (<75%) groups based on the degree of epiboly completed (left) and quantified (right). Co-injecting *fdh* mRNA or *fdh* N-ter-mRNA with *fdh* MO partially rescued the delayed epiboly. Incubating morphants with 0.25 mM THF or 20 μM N-acetyl-L-cysteine (NAC) partially rescued delayed epiboly. For rescuing, morphants were either co-injected with fdh mRNA (400 pg) or incubated in water containing rescuing agents (0.25 mM THF or 20 μM N-acetyl-L-cysteine (NAC)) 2 h after MO injection. (C) Embryos at the stages of 65%–70% epiboly were fixed, stained with rhodamine phalloidin for F-actin and imaged with confocal microscope. Local actin recruitment in the yolk syncytial layer (white arrow) was significantly diminished in *fdh* morphants; whereas clearly observed in control and RNA-rescued morphants. (D) Embryos injected with *fdh* MO with/without rescuing agents were characterized for lateral line formation with 4-Di-2-ASP staining at 3-dpf and categorized into normal, mild and severe group based on the presence/absence and migratory extent of lateral line neuromasts (left). Displaced neuromasts (arrowhead) and lack of neuromast were often seen in *fdh* morphants. Images were taken using Leica Z16 APO fluorescence dissecting microscope. The percentage of embryos in each phenotypic category was quantified for each experimental group (right). MO, *fdh* morphants; L1–6: neuromasts lined up along the flanks of embryos; ter: neuromasts clustered at the tail region; f-R, fdh full-length mRNA; fN-R, fdh N-terminal domain mRNA.

4. Discussion

FDH, the most abundant folate enzyme in the liver, has been considered a potential chemotherapeutic target. However, lacking the knowledge on the biological significance of FDH under normal physiological conditions has hampered the development of anti-folate drug targeting FDH. Here, we investigated the significance of FDH in embryogenesis by knocking down *fdh* expression in zebrafish embryos. We showed that decreasing *fdh* expression decreased the embryonic THF level and increased oxidative stress, leading to impeded cell migration, delayed epiboly, obstructed convergent extension and subsequently developmental anomalies. The malformed notochord, somite and heart observed in morphants (Figs. 2, 3 and 4) also supported the importance of proper actin dynamic for the notochord and heart development [41,42]. It should be noted that the *fdh* expression we knocked-down was likely the cytosolic form of FDH, judging from the high similarity of its primary structures and biochemical properties to those of mammalian FDHs. The current studies provide in vivo evidence for the functions of FDH in modulating folate pools and embryogenesis.

Our data suggested that the anti-oxidative activity of FDH was crucial for embryogenesis. Previous studies suggested that FDH played a role in embryonic development because *fdh* was expressed in the post-natal and adult mice cerebellum [11,43]. We found that knocking down *fdh* expression disturbed the development of various embryonic tissues, including neural tissues, which was accompanied by decreased BrdU incorporation and increased apoptotic signals (Supplement 8). The C2 and C8 of 10-formyl-THF are required for purine de novo biosynthesis. One would expect that the impact to embryogenesis caused by increased or decreased FDH would be due to the effect to 10-formyl-THF level. Unexpectedly, we found no appreciable change in embryonic 10-formyl-THF level when embryos were injected with either *fdh* mRNA or morpholino oligonucleotides. Instead, we detected fluctuation of THF levels in the wake of altered *fdh* expression. Previous studies showed that in rapidly proliferating tumor cells FDH was down-regulated. In contrast, in regenerating the liver, which was also full of rapidly proliferating cells, FDH was highly expressed [44]. These data, together with our observation that overexpressing FDH did not cause obvious abnormality in embryos, suggested that there might not be a direct causal relationship between FDH expression and nucleotide biosynthesis in proliferating cells/tissues. Mechanisms besides disturbing nucleotide biosynthesis may play a role in the obstructed embryogenesis observed in FDH morphants. Further studies showed that the increased oxidative stress due to decreased THF level caused by *fdh* knockdown contributed at least partly to the abnormality in morphants. Oxidative stress occurs when the steady-state balance between pro-oxidants and anti-oxidants is changed. THF possesses anti-oxidative

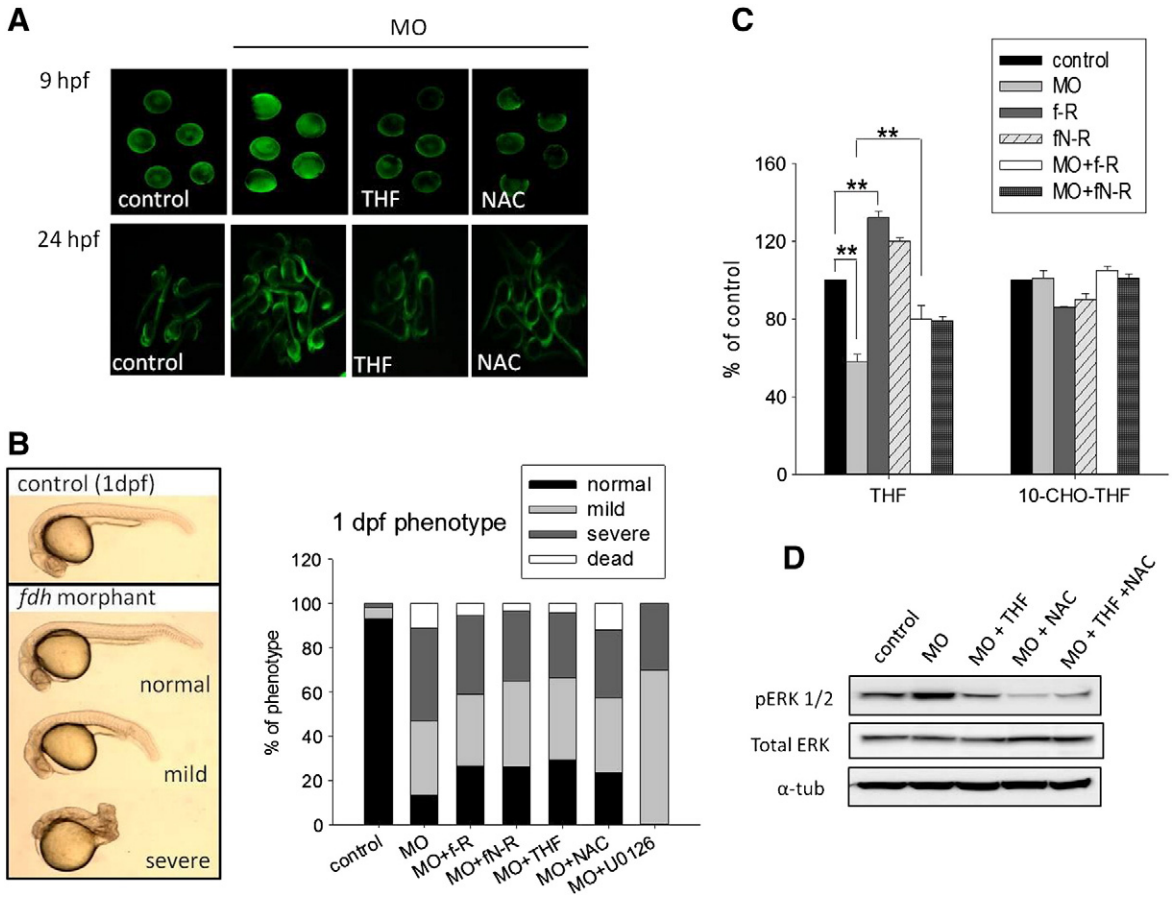

Fig. 6. Knocking-down fdh expression induced oxidative stress and ERK phosphorylation. (A) Control embryos and embryos injected with *fdh* MO (f-MO) were stained with DCFDA for ROS detection at 9 hpf (upper) and 24 hpf (lower). THF, NAC and U0126, and a pERK inhibitor were added to embryo water 2 h after MO injection and removed before DCFDA staining. (B) The phenotypes of morphants with/without rescuing treatment at 1 dpf were categorized into normal, mild and severe groups based on the severity of morphological anomalies (left) and quantified (right). (C) The content of THF and 10-formyl-THF in *fdh* morphants with/without RNA rescue was measured with HPLC and compared with control embryos. (D) Both control embryos and *fdh* morphants at 1 dpf were collected for Western blotting to examine ERK expression and phosphorylation. Total embryos extract (40 μg) was loaded on each lane for SDS-PAGE. MO, *fdh*-morphants; NAC, N-acetyl-cysteine; *, $p < 0.05$; **, $p < 0.01$ Statistic significance was calculated with Student's t-test.

activity and is stabilized by binding to the N-terminal domain of FDH [7,39]. Increased FDH has been shown to help relieve oxidative stress-induced by ethanol exposure [40]. The reversal of morphogenetic abnormalities by adding THF or NAC confirmed the causal effects of oxidative stress in the *fdh*-knockdown induced pathogenesis and further supported the significance of the anti-oxidative activity provided by FDH during embryogenesis.

Although the physiological significance of the FDH N-terminal domain hydrolase activity remains elusive we were able to reverse the abnormalities of morphants by co-injecting the mRNA encoding only the FDH N-terminal domain. Our results suggest that the function of the FDH N-terminal domain maybe for maintaining the intracellular THF level. 10-Formyl-THF dehydrogenase activity results in the reduction of one-carbon units by generating carbon dioxide; whereas hydrolase activity results in the storage of one-carbon units as formate. Therefore, the significance of FDH hydrolase activity, if it exists in vivo, would be important since it would lead to the production of formate instead of carbon dioxide. We have expressed, purified, crystallized and done preliminary structural analysis of the zebrafish N-terminal domain in the presence of THF. There are at least two sites where THF is bound (unpublished data). We are in the process of making site mutants to determine the possible catalytic site and the tight binding non-catalytic site. These mutants will be tested to see if they still can partially restore normal function in our *fdh* knock down mutants.

The constant level of 10-formyl-THF in embryos regardless of increased or decreased *fdh* expression also suggests that other enzyme(s) or mechanism(s) might be responsible for maintaining a steady level of 10-formyl-THF in zebrafish embryos. Curiously, this postulated mechanism(s) seems to be lost in evolution since both decreased THF and increased 10-formyl-THF were observed in the NEUT 2 mice lacking FDH activity [12]. The question thus arises as what other mechanism guards the intracellular 10-formyl-THF level and keeps it constant in zebrafish embryos, since altered FDH expression did not affect it. The activity of 10-formyltetrahydrofolate synthase catalyzes the formation of 10-formylTHF from THF, ATP and formate. These two enzymes form a "futile cycle" in cells. The importance of 10-formyltetrahydrofolate synthase has been recently addressed in mouse models, in which impeded pregnancy and embryogenesis occurred due to disturbed purine synthesis in mice lacking 10-formyltetrahydrofolate synthase activity [45,46]. It shall be interesting and central to explore the possibility of 10-formyltetrahydrofolate synthase acting in counterbalance of FDH to maintain a constant intracellular 10-formyl-THF level.

Our results showed that *fdh* knockdown interfered with the later stage of cardiac development. Distinct ventricle and atrium chambers were observed in morphants, indicating that the fusion of the myocardial precursor and elongation of heart tube along the midline occurred properly. However, the initial leftward placement of the elongated heart tube and subsequent gradual bending at the atrioventricular boundary was unsuccessful. Both severe pericardial edema and significantly slowed heart rate could be embryonic lethal if occurred in mammals. Previous studies showed that homozygous NEUT2 mice lacking FDH were viable, fertile and showed no increased incidence of neural

tube defects, but required extended breeding time to produce offspring (>200 days in NEUT2 mice vs. ~30 days in normal control). This reproductive deficiency was attributed to increased fetal lethality probably resulting from early arrest of fetal development after implantation [12]. It should be noted that the impacts of a defective cardiac system to the developing mouse embryos and to zebrafish larvae shall be dissimilar. A functional circulation system is indispensable for mammalian embryonic development. Nevertheless, a functional circulation system is not essential for zebrafish larvae before 7 dpf since the transport of nutrient and oxygen can be accomplished by diffusion. That means that miscarriage would occur to most of the mouse embryos with defective hearts in very early stages of gestation, even before the awareness of conception. Only very few embryos, probably with unidentified mutation for adaption, could survive and be born. Contrarily, zebrafish larvae with defective hearts could still survive for one week to be observed and recorded. This was in agreement with the low survival rate (~10%) observed in our *fdh* morphants (Figs. 2, 5 and 6) in which all those morphants with either mild or severe phenotypic abnormalities were dead by 1 week post fertilization. Our results provide a possible explanation for the reproductive defect observed in the mice lacking active FDH.

Disparities were found between our studies and other reports. We showed that decreasing *fdh* expression impeded actin recruitment at the migratory frontier of the enveloping layer in the blastoderm and delayed epiboly progression. These results are in agreement with the observation that disrupting actin-based structures led to the slowing or immediate arrest of epiboly and support the importance of actin dynamics within the YSL and EVL during embryogenesis [36]. They also support the involvement of FDH in actin dynamic control. However, it was the increase, instead of decrease, of FDH that inhibited actin dynamic and cell mobility in human lung adenocarcinoma epithelial cells [47]. Also, high levels of FDH exerted no harmful effect in zebrafish embryos and regenerating liver; whereas suppressor activity was reported for FDH when overexpressed in cancer cells [15,44]. In addition, we observed severely impeded embryonic development in *fdh* knockdown embryos; whereas in a mouse model, lacking FDH activity did not elicit obvious morphological abnormality except extended breeding time [12]. These differences probably reflect the divergence among different experimental platforms. They also imply that there exist distinct functions and regulatory mechanisms for FDH in different tissues and under different circumstances and that our understanding on the role of FDH is incomplete. Further investigation on the mechanisms underlying these differences may help elucidate the conserved biological functions of FDH during evolution and in disease pathogenic processes.

In the current study, we reported that pERK was activated in response to the oxidative stress that resulted from decreased THF levels. Previous studies showed that the binding of folic acid to folate receptors on cell membrane inhibited HUVEC proliferation via activating cSrc/ERK 2/NF-κB/p53 signaling pathway and inhibited cell migration through inhibiting cSrc/p190RhoGAP-signaling pathway [48,49]. We do not know whether the folic acid-induced inhibition on HUVEC migration also involves intervention to one-carbon metabolism since the intracellular folate contents in those folic acid-exposed cells were not reported. The question whether comparable or overlapping mechanisms occurred in both *fdh* morphants and folic acid-treated cells warrants further investigation.

Supplementary data to this article can be found online at http://dx.doi.org/10.1016/j.bbagen.2014.04.009.

Author contribution

WNC, YHC, BHC, HJT and TFF conceived and designed the experiments. WNC, GHL, TTK, CYL, THH, JNT and HRW performed the experiments. WNC and TFF analyzed the data and wrote the manuscript.

References

[1] A.E. Czeizel, I. Dudas, A. Vereczkey, F. Banhidy, Folate deficiency and folic acid supplementation: the prevention of neural-tube defects and congenital heart defects, Nutrients 5 (2013) 4760–4775.
[2] D. Schirch, E. Villar, B. Maras, D. Barra, V. Schirch, Domain structure and function of 10-formyltetrahydrofolate dehydrogenase, J. Biol. Chem. 269 (1994) 24728–24735.
[3] H. Donato, N.I. Krupenko, Y. Tsybovsky, S.A. Krupenko, 10-Formyltetrahydrofolate dehydrogenase requires a 4′-phosphopantetheine prosthetic group for catalysis, J. Biol. Chem. 282 (2007) 34159–34166.
[4] R.J. Cook, R.S. Lloyd, C. Wagner, Isolation and characterization of cDNA clones for rat liver 10-formyltetrahydrofolate dehydrogenase, J. Biol. Chem. 266 (1991) 4965–4973.
[5] W.N. Chang, H.C. Lin, T.F. Fu, Zebrafish 10-formyltetrahydrofolate dehydrogenase is similar to its mammalian isozymes for its structural and catalytic properties, Protein Expr. Purif. 72 (2010) 217–222.
[6] A.A. Chumanevich, S.A. Krupenko, C. Davies, The crystal structure of the hydrolase domain of 10-formyltetrahydrofolate dehydrogenase: mechanism of hydrolysis and its interplay with the dehydrogenase domain, J. Biol. Chem. 279 (2004) 14355–14364.
[7] T.F. Fu, B. Maras, D. Barra, V. Schirch, A noncatalytic tetrahydrofolate tight binding site is on the small domain of 10-formyltetrahydrofolate dehydrogenase, Arch. Biochem. Biophys. 367 (1999) 161–166.
[8] C. Kutzbach, E.L. Stokstad, Partial purification of a 10-formyl-tetrahydrofolate: NADP oxidoreductase from mammalian liver, Biochem. Biophys. Res. Commun. 30 (1968) 111–117.
[9] M.C. Anguera, M.S. Field, C. Perry, H. Ghandour, E.P. Chiang, J. Selhub, B. Shane, P.J. Stover, Regulation of folate-mediated one-carbon metabolism by 10-formyltetrahydrofolate dehydrogenase, J. Biol. Chem. 281 (2006) 18335–18342.
[10] D.W. Kim, T. Huang, D. Schirch, V. Schirch, Properties of tetrahydropteroylpentaglutamate bound to 10-formyltetrahydrofolate dehydrogenase, Biochemistry 35 (1996) 15772–15783.
[11] T.E. Anthony, N. Heintz, The folate metabolic enzyme ALDH1L1 is restricted to the midline of the early CNS, suggesting a role in human neural tube defects, J. Comp. Neurol. 500 (2007) 368–383.
[12] K.M. Champion, R.J. Cook, S.L. Tollaksen, C.S. Giometti, Identification of a heritable deficiency of the folate-dependent enzyme 10-formyltetrahydrofolate dehydrogenase in mice, Proc. Natl. Acad. Sci. U. S. A. 91 (1994) 11338–11342.
[13] L.A. Hoeferlin, B. Fekry, B. Ogretmen, S.A. Krupenko, N.I. Krupenko, Folate stress induces apoptosis via p53-dependent de novo ceramide synthesis and up-regulation of ceramide synthase 6, J. Biol. Chem. 288 (2013) 12880–12890.
[14] S. Ghose, N.V. Oleinik, N.I. Krupenko, S.A. Krupenko, 10-Formyltetrahydrofolate dehydrogenase-induced c-Jun-NH2-kinase pathways diverge at the c-Jun-NH2-kinase substrate level in cells with different p53 status, Mol. Cancer Res. 7 (2009) 99–107.
[15] N.V. Oleinik, N.I. Krupenko, D.G. Priest, S.A. Krupenko, Cancer cells activate p53 in response to 10-formyltetrahydrofolate dehydrogenase expression, Biochem. J. 391 (2005) 503–511.
[16] W.N. Chang, J.N. Tsai, B.H. Chen, T.F. Fu, Cloning, expression, purification, and characterization of zebrafish cytosolic serine hydroxymethyltransferase, Protein Expr. Purif. 46 (2006) 212–220.
[17] W.N. Chang, J.N. Tsai, B.H. Chen, H.S. Huang, T.F. Fu, Serine hydroxymethyltransferase isoforms are differentially inhibited by leucovorin: characterization and comparison of recombinant zebrafish serine hydroxymethyltransferases, Drug Metab. Dispos. Biol. Fate Chem. 35 (2007) 2127–2137.
[18] T.T. Kao, K.C. Wang, W.N. Chang, C.Y. Lin, B.H. Chen, H.L. Wu, G.Y. Shi, J.N. Tsai, T.F. Fu, Characterization and comparative studies of zebrafish and human recombinant dihydrofolate reductases—inhibition by folic acid and polyphenols, Drug Metab. Dispos. 36 (2008) 508–516.
[19] T.T. Kao, G.H. Lee, C.C. Fu, B.H. Chen, L.T. Chen, T.F. Fu, Methotrexate-induced decrease in embryonic 5-methyl-tetrahydrofolate is irreversible with leucovorin supplementation, Zebrafish 10 (2013) 326–337.
[20] T.T. Kao, W.N. Chang, H.L. Wu, G.Y. Shi, T.F. Fu, Recombinant zebrafish {gamma}-glutamyl hydrolase exhibits properties and catalytic activities comparable with those of mammalian enzyme, Drug Metab. Dispos. 37 (2009) 302–309.
[21] P. Chuankhayan, T.T. Kao, C.C. Lin, H.H. Guan, A. Nakagawa, T.F. Fu, C.J. Chen, Structural insights into the hydrolysis and polymorphism of methotrexate polyglutamate by zebrafish gamma-glutamyl hydrolase, J. Med. Chem. 56 (19) (Oct 10 2013) 7625–7635.
[22] M. Westerfield, The Zebrafish Book: Guide for the Laboratory Use of Zebrafish (*Danio rerio*), University of Oregon Press, Eugene, 2007.
[23] C.B. Kimmel, W.W. Ballard, S.R. Kimmel, B. Ullmann, T.F. Schilling, Stages of embryonic development of the zebrafish, Dev. Dyn. 203 (1995) 253–310.
[24] V. Link, A. Shevchenko, C.P. Heisenberg, Proteomics of early zebrafish embryos, BMC Dev. Biol. 6 (2006) 1.
[25] T. Jowett, Double in situ hybridization techniques in zebrafish, Methods 23 (2001) 345–358.
[26] C. Thisse, B. Thisse, T.F. Schilling, J.H. Postlethwait, Structure of the zebrafish snail1 gene and its expression in wild-type, spadetail and no tail mutant embryos, Development 119 (1993) 1203–1215.
[27] H.W. Detrich 3rd, M.W. Kieran, F.Y. Chan, L.M. Barone, K. Yee, J.A. Rundstadler, S. Pratt, D. Ransom, L.I. Zon, Intraembryonic hematopoietic cell migration during vertebrate development, Proc. Natl. Acad. Sci. U. S. A. 92 (1995) 10713–10717.
[28] H. Grandel, J. Kaslin, J. Ganz, I. Wenzel, M. Brand, Neural stem cells and neurogenesis in the adult zebrafish brain: origin, proliferation dynamics, migration and cell fate, Dev. Biol. 295 (2006) 263–277.

[29] T. Idziorek, J. Estaquier, F. De Bels, J.C. Ameisen, YOPRO-1 permits cytofluorometric analysis of programmed cell death (apoptosis) without interfering with cell viability, J. Immunol. Methods 185 (1995) 249–258.
[30] O. Anichtchik, H. Diekmann, A. Fleming, A. Roach, P. Goldsmith, D.C. Rubinsztein, Loss of PINK1 function affects development and results in neurodegeneration in zebrafish, J. Neurosci. 28 (2008) 8199–8207.
[31] C. Anastasaki, K.A. Rauen, E.E. Patton, Continual low-level MEK inhibition ameliorates cardio-facio-cutaneous phenotypes in zebrafish, Dis Model Mech, 5 546-552
[32] A. Chakraborty, T. Uechi, S. Higa, H. Torihara, N. Kenmochi, Loss of ribosomal protein L11 affects zebrafish embryonic development through a p53-dependent apoptotic response, PLoS.One 4 (2009) e4152.
[33] A. Nasevicius, S.C. Ekker, Effective targeted gene 'knockdown' in zebrafish, Nat. Genet. 26 (2000) 216–220.
[34] C.J. Huang, C.T. Tu, C.D. Hsiao, F.J. Hsieh, H.J. Tsai, Germ-line transmission of a myocardium-specific GFP transgene reveals critical regulatory elements in the cardiac myosin light chain 2 promoter of zebrafish, Dev. Dyn. 228 (2003) 30–40.
[35] S.E. Zalik, E. Lewandowski, Z. Kam, B. Geiger, Cell adhesion and the actin cytoskeleton of the enveloping layer in the zebrafish embryo during epiboly, Biochem. Cell Biol. Biochim. Biol. Cell. 77 (1999) 527–542.
[36] J.C. Cheng, A.L. Miller, S.E. Webb, Organization and function of microfilaments during late epiboly in zebrafish embryos, Dev. Dyn. 231 (2004) 313–323.
[37] W.K. Metcalfe, C.B. Kimmel, E. Schabtach, Anatomy of the posterior lateral line system in young larvae of the zebrafish, J. Comp. Neurol. 233 (1985) 377–389.
[38] W.K. Metcalfe, Sensory neuron growth cones comigrate with posterior lateral line primordial cells in zebrafish, J. Comp. Neurol. 238 (1985) 218–224.
[39] B.M. Rezk, G.R. Haenen, W.J. van der Vijgh, A. Bast, Tetrahydrofolate and 5-methyltetrahydrofolate are folates with high antioxidant activity. Identification of the antioxidant pharmacophore, FEBS Lett. 555 (2003) 601–605.
[40] T.H. Hsiao, C.J. Lin, Y.S. Chung, G.H. Lee, T.T. Kao, W.N. Chang, B.H. Chen, J.J. Hong, T.F. Fu, Ethanol-induced up-regulation of 10-formyltetrahydrofolate dehydrogenase helps relieve ethanol-induced oxidative stress, Mol. Cell. Biol. 34 (3) (Feb 2014) 498–509.
[41] J. Prudent, N. Popgeorgiev, B. Bonneau, J. Thibaut, R. Gadet, J. Lopez, P. Gonzalo, R. Rimokh, S. Manon, C. Houart, P. Herbomel, A. Aouacheria, G. Gillet, Bcl-wav and the mitochondrial calcium uniporter drive gastrula morphogenesis in zebrafish, Nat. Commun. 4 (2013) 2330.
[42] M.C. Danos, H.J. Yost, Role of notochord in specification of cardiac left–right orientation in zebrafish and Xenopus, Dev. Biol. 177 (1996) 96–103.
[43] S.G. Kuhar, L. Feng, S. Vidan, M.E. Ross, M.E. Hatten, N. Heintz, Changing patterns of gene expression define four stages of cerebellar granule neuron differentiation, Development 117 (1993) 97–104.
[44] S.A. Krupenko, N.V. Oleinik, 10-Formyltetrahydrofolate dehydrogenase, one of the major folate enzymes, is down-regulated in tumor tissues and possesses suppressor effects on cancer cells, Cell Growth Differ. 13 (2002) 227–236.
[45] J. Momb, J.P. Lewandowski, J.D. Bryant, R. Fitch, D.R. Surman, S.A. Vokes, D.R. Appling, Deletion of Mthfd1l causes embryonic lethality and neural tube and craniofacial defects in mice, Proc. Natl. Acad. Sci. U. S. A. 110 (2013) 549–554.
[46] K.E. Christensen, L. Deng, K.Y. Leung, E. Arning, T. Bottiglieri, O.V. Malysheva, M.A. Caudill, N.I. Krupenko, N.D. Greene, L. Jerome-Majewska, R.E. MacKenzie, R. Rozen, A novel mouse model for genetic variation in 10-formyltetrahydrofolate synthetase exhibits disturbed purine synthesis with impacts on pregnancy and embryonic development, Hum. Mol. Genet. 22 (2013) 3705–3719.
[47] N.V. Oleinik, N.I. Krupenko, S.A. Krupenko, ALDH1L1 inhibits cell motility via dephosphorylation of cofilin by PP1 and PP2A, Oncogene 29 (2010) 6233–6244.
[48] T.C. Hou, J.J. Lin, H.C. Wen, L.C. Chen, S.P. Hsu, W.S. Lee, Folic acid inhibits endothelial cell migration through inhibiting the RhoA activity mediated by activating the folic acid receptor/cSrc/p190RhoGAP-signaling pathway, Biochem. Pharmacol. 85 (3) (Feb 2013) 376–384.
[49] S.Y. Lin, W.R. Lee, Y.F. Su, S.P. Hsu, H.C. Lin, P.Y. Ho, T.C. Hou, Y.P. Chou, C.T. Kuo, W.S. Lee, Folic acid inhibits endothelial cell proliferation through activating the cSrc/ERK 2/NF-kappaB/p53 pathway mediated by folic acid receptor, Angiogenesis 15 (2012) 671–683.